3D GEOLOGICAL MODELLING AND GEOTHERMAL ASSESSMENT OF THE LIMAGNE BASIN (FRANCE) Z-99

P. Calcagno [(*)], C. Baujard [(**)], A. Dagallier [(*)], L. Guillou-Frottier [(*)], A. Genter [(***)], T. Kohl [(**)], G. Courrioux [(*)]

[(*)]*BRGM, 3 avenue C. Guillemin – 45060 Orléans (France)*
[(**)]*Geowatt, Dohlenweg 28 – 8050 Zürich (Switzerland)*
[(***)]*EEIG Exploitation Minière de la Chaleur, Route de Soultz - 67250 Kutzenhausen (France)*

Summary

This work consists in assessing the geothermal potential of the Limagne area (Massif Central, France) in 3D by building a geological model and computing a thermal model. This reservoir is a Tertiary graben belonging to West European rift system characterized by a geothermal anomaly with Tertiary clastic reservoirs. In order to better understand the geometry of geology, various geological and geophysical data acquired during various campaigns are re-interpreted to construct a coherent 3D model. The new interpretation consists in a 35km x 30km x 5km geological model extending from the basement to the surface of the basin. The geometry is then used to constrain a numerical model (assuming a diffusive temperature regime) based on the thermal conductivity of the various geological units and thermal boundary conditions. The total amount of geothermal energy available for each aquifer is computed, and the geothermal potential i.e. the recoverable energy, is mapped over the entire model.

Geological setting

The Limagne d'Allier basin is located in an area where the temperature extrapolated at 5 km depth is high (see Figure 1). The area has been studied for its geothermal potential based on clastic reservoirs overlying the basement rocks (Genter et al., 2003).

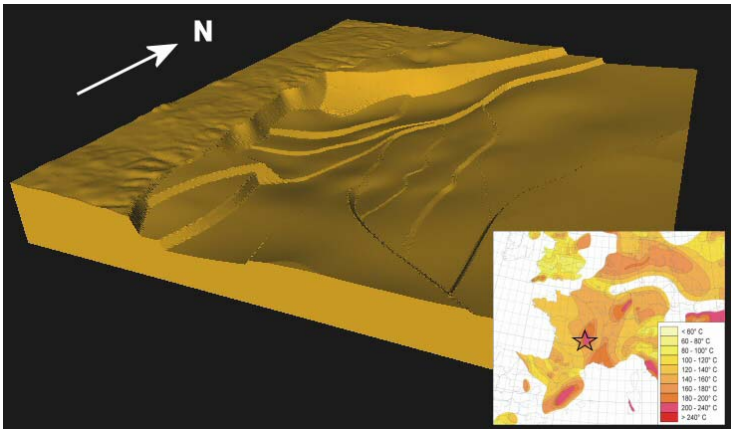

Figure 1: View to the NW of the basement below the Limagne Basin, illustrating the network of faults used to model the basement structure (model dimensions: 30 km x 35 km x 5 km). The geometry of the basement was modelled by taking into account field geology observations, seismic sections and boreholes together with a basement surface derived from gravimetric inversion. The location map shows contours of temperature extrapolated to 5 km depth (Hurtig et al., 1991); the Limagne Basin project (star) is located in an area of anomalously high temperature.

Located north of Clermont-Ferrand, France, this NNE to NS oriented Tertiary basin is bounded by regional normal faults. From Upper Eocene to Oligocene, a graben formed due to progressive subsidence resulting from the extension phase affecting the West-European plate during Oligocene. The Limagne basin is delimited by the N-S Clermont-Ferrand fault in the east and by the NE-SW Aigueperse fault in the north. Both faults have a normal throw of several hundred metres, with a strike slip component for the Aigueperse fault. The combination of those two faults delineates the deepest part of the basin situated around Riom city. Based on seismic lines interpretation, most of the faults inside the basin had no activity after the Oligocene. The two main faults, however, do show evidence of later movement. Overlying the Limagne d'Allier basement, four main sedimentary sequences fill the basin: Middle Eocene (S1), Upper Eocene (S2), Rupelian (S3) and Chattian (S4). Each sequence is composed of a sedimentary cycle ranging from detrital

formations at the base ("Reservoir"), followed by alternating layers of detrital and carbonate sediments (“Intermediate”), and capped by formations of marls and carbonates at the top (“Top”).

3D Geological modelling

Within the Allier basin, the geology of about 100 old wells has been reinterpreted in terms of lithofacies and sequential stratigraphy. A database with the thickness of each lithofacies has been constructed and used for the geometrical modeling. In this area, several seismic campaigns have been done for oil and uranium exploration between 1958 and 1979. For this study, 26 old seismic profiles have been calibrated on borehole data, digitized and reprocessed through specific seismic software. A reinterpretation of these seismic lines has been performed and 3 main geological interfaces acting as seismic reflectors were mapped as well as a series of normal faults.
The geological model is constructed using the potential field interpolation method (Calcagno et al., in press). The limits between the formations and dips measurement measured in the field and interpreted from the geological and geophysical data are used to achieve a coherent 3D interpretation. The resulting model infers the geological formation at any point of the 3D space. The geological interfaces derived from isovalues of the interpolated potential field. A *geological pile* describes the history of the geological events to manage to topology of the model (Figure 2c). The *geological pile* is composed of a set of geological formations, chronologically ordered, and gathered together in interacting *series*. Each *series* is interpolated using a single potential field.

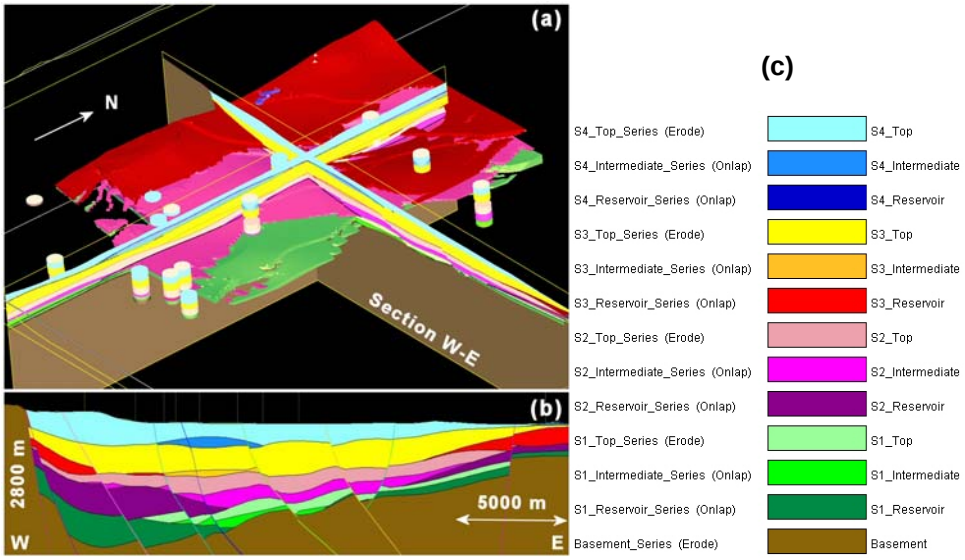

Figure 2: View of the Limagne Basin geology model (30 km x 35 km x 5 km).
(a) 3D view from S-E of the 4 detrital formations (“Reservoir”) volumes in the central part of the model. Boreholes in the area are shown, and two cross-sections (S-N and W-E).
(b) W-E section of the whole basin.
(c) Geological *pile* derived from the broad geological knowledge of the basin. Four sedimentary sequences (S1 to S4) are deposited on top of the basement ("Basement"). Each sequence is divided into three depositional phases (“Reservoir”, “Intermediate” and “Top”). The sequences are separated by erosional surfaces (*Erode* relation for the top series of the four sequences). Each formation is modelled using independent potential fields because the variability of thickness is not correlated from a formation to another.

In order to model the erosional surfaces that define top of each sedimentary cycle, the top of marls and carbonates for each sequence is assigned to an *Erode* relationship. The thickness of each formation varies both spatially and temporally. The "Reservoir" formations are thicker along the basin-margins than in the centre of the basin. The "Intermediate" formations correspond to a transitional environment, and lacustrine carbonate formations are thicker in the central, deeper part of the basin. Since the thickness variability is not correlated from one formation to another within the same sequence, their interfaces cannot be represented by isovalues of a single potential field. Consequently, each formation must be modelled with an independent potential field, i.e. each formation must belong to an independent *series* (Figure 2c).
The faults bordering the basin and interacting with the sedimentary formation are modelled through drift functions impacting the potential field interpolation (Calcagno et al., in press). They are gathered into a fault network managing

the topology of the interaction between faults and between faults and *series*. Figure 1 shows the geometry of the basement built using a fault network.
The complete resulting model is illustrated in Figure 2 showing a 3D view of the "Reservoir" formations, some boreholes and two orthogonal sections (Figure 2a), and a W-E section of the whole basin (Figure 2b). The modelled cross-section demonstrates (i) how the fault network controls the fault system geometry, (ii) the outcomes of the *Onlap* or *Erode* rock relationships, and (iii) the implications of the relations between faults and series.

Meshing of the geological model

The geological layers were discretized using hexahedra and prisms (3D elements). Faults were discretized using squares and triangles (2D elements). A Finite Element mesh was built using the Winfra mesh generator and the Orion extension. Both tools were internally developed in GEOWATT AG. The resulting mesh is an unstructured mesh composed of more than 100'000 elements. The basement and a suite of 4 sedimentary units (defined by top of S1, top of S2, top of S3 and topography) were taken in account into the mesh. The faults are modelled as 2D elements, implying the use of a thickness parameter. Most of the faults are taken in account in the mesh. Most of them were assumed as vertical, except two of them. These two faults were manually meshed in 3D in order to respect at best their diping. Figure 3 shows in detail the obtained mesh.

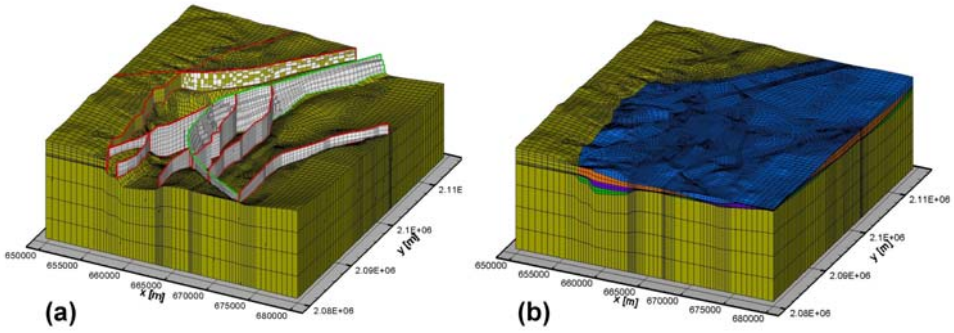

Figure 3: Views of the Limagne Finite Element Mesh adapted from the geology model
(a) 3D view of the basement and of the faults
(b) 3D view of the basement and of the formations S1, S2, S3 and S4 (from bottom to top).

3D Thermal modelling

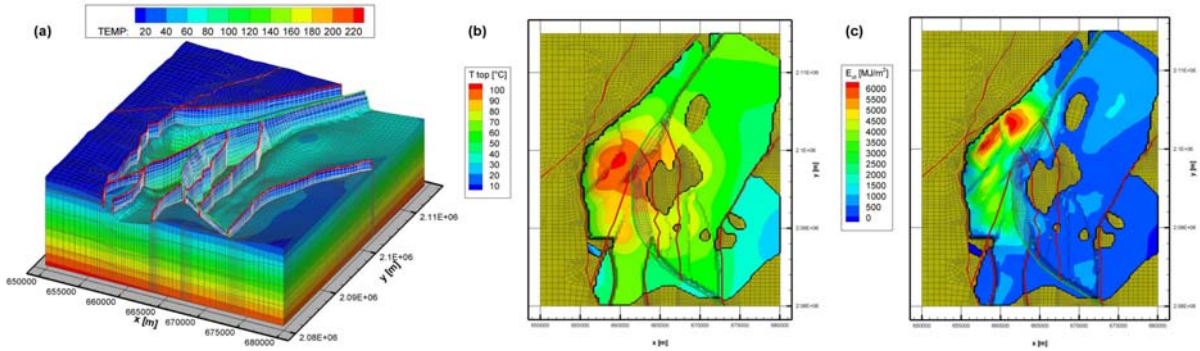

Figure 4: Computation results of the numerical simulation.
(a) 3D temperature distribution in the Basement and in the faults.
(b) Temperature extracted at the top of the Reservoir S1.
(c) Geothermal potential E_{ut} [MJ·m^{-2}] computed in the Reservoir S1.

A diffusive thermal numerical model is realised (therefore assuming that water movements are too weak to play an important role in the temperature distribution into the model). Two boundary conditions are used: a Dirichlet boundary condition (T imposed , 10°C, fixed) is set at the surface of the model (topography), and a Neumann boundary condition (imposed flux, 105 mW·m^{-2}, after calibration) is set at the bottom of the model. The other lateral boundaries are

insulating. The simulation is run steady-state, neglecting effects of passed climate change or transitory effects in the sediments. The best fit on the thermal data (only one borehole temperature profile could be taken in account) was obtained with realistic values of thermal conductivities (between 2 $W \cdot m^{-1} \cdot K^{-1}$ and 3 $W \cdot m^{-1} \cdot K^{-1}$) and radiogenic heat production ($3.0 \cdot 10^{-6}$ $W \cdot m^{-3}$ for the basement and $0.5 \cdot 10^{-6}$ $W \cdot m^{-3}$ for the sedimentary layers). The values are much closed to what was derived from sample and core analysis (Dagallier, 2004). The temperature is then calculated in the 3D numerical model, and extracted at the top of the aquifers that could potentially represent interesting targets for a geothermal exploitation (Figure 4).

Geothermal potential

The total amount of geothermal energy available is then computed and mapped in each potential reservoir S1, S2 and S3, according to the following parameters:

- Thickness and extension of the aquifer derived from the geological model,
- Temperature distribution derived from the numerical model,
- Reinjection temperature (assumed 30°C) and heat capacity of the host rock.

This entire energy cannot be exploited. The geothermal potential is defined by the amount of recoverable energy of the medium. The recovery factor is defined by the ratio between the geothermal potential and the available energy. In the following, a recovery factor of 5 % is assumed in order to compute the geothermal potential of each aquifer. This factor should vary as function of porosity and hydraulic conductivity of each aquifer. Previous resource analysis showed that a recovery factor of 5 % could be considered a realistic value (Signorelli and Kohl, 2006). The geothermal potential was computed and mapped for every aquifer S1, S2 and S3 (example of the geothermal potential of reservoir S1: see Figure 4c).

Conclusion

Works performed showed a full approach to quantify the geothermal potential of a region, from the geological modelling to the mapping of the potential. As a result, the deepest reservoir, which is consequently the hottest, and also the thickest, is the most interesting target for a geothermal exploitation. The zones of greatest interest were localised. Results obtained could be enhanced by better temperature information on the domain and by taking in account the permeability of the reservoirs into the computation of the recovery factor.

Acknowledgement

This work is supported by ADEME (French Agency for Energy and Environment) and benefits from the ENGINE European coordination action (Enhanced Geothermal Innovative Network for Europe, http://engine.brgm.fr).

REFERENCES

- Calcagno P., Courrioux G., Guillen A., Chilès J.P., *Geological modelling from field data and geological knowledge, Part I – Modelling method coupling 3D potential-field interpolation and geological rules.* Physics of the Earth and Planetary Interiors, in press.
- *Dagallier*, A., 2004: *Assessment of Geothermal Energy Potential of the Tertiary Limagne Basin (France)*, Technical University of Denmark.
- Genter A., Giot D., Lieutenant N., Nehlig P., Rocher Ph., Roig J.Y., Chevremont Ph., Guillou-Frottier L., Martelet G., Bitri A., Perrin J., Serrano O., Courtois N., Vigouroux Ph., Négrel Ph., Serra H., Petelet-Giraud E., 2003: *Méthodologie de l'inventaire géothermique des Limagnes. Compilation des données.* BRGM Open File report, R52644, 122 p.
- Hurtig, E., Cermak, V., Haenel, R., Zui, V., 1991: *Geothermal Atlas of Europe: Hermann Haack* Verlagsgesellshaft. 156 pp.
- Signorelli, S. and Kohl, T., 2006: *Geothermischer Ressourcenatlas der Nordschweiz - Gebiet des nördlichen Schweizer Mittellandes*, Schweizerische Geophysikalische Kommission